DOI 10.1007/s11595-017-1724-5

# Deformation Behavior and Formability of Gradient Nano-grained AISI 304 Stainless Steel Processed by Ultrasonic Impact Treatment

**YANG Xinjun[1], LING Xiang[2], WANG Dongxiang[1], WANG Wei[3,4,5*]**

*(1. Jiangsu Key Laboratory of Advanced Food Manufacturing Equipment & Technology, School of Mechanical Engineering, Jiangnan University, Wuxi 214122, China; 2. Jiangsu Key Laboratory of Process Enhancement and New Energy Equipment Technology, School of Mechanical and Power Engineering, Nanjing Tech University, Nanjing 211816, China; 3.School of Automotive Engineering, Wuhan University of Technology, Wuhan 430070, China; 4.Hubei Province Key Laboratory of Modern Automotive Technology, Wuhan 430070, China; 5.Hubei Province Automotive Parts Synergy Innovation Center, Wuhan 430070, China)*

**Abstract:** The deformation behavior and formability of gradient nano-grained (GNG) AISI 304 stainless steel in uniaxial and biaxial states were investigated by means of tensile test and small punch test (SPT). The GNG top layer was fabricated on coarse grains (CG) AISI 304 by ultrasonic impact treatment. The results showed that the CG substrate could effectively suppress the strain localization of NC in GNG layer, and an approximate linear relationship existed between the thickness of substrate ($h$) and uniform true strain before necking ($\varepsilon_{unif}$). Grain growth of NC was observed at the stress state with high Stress triaxiality $T$, which led to better ductility of GNG/CG 304 in SPT, as well as similar true strain after the onset of necking ($\varepsilon_{neck}$) compared with coarse 304 in tensile test. Ei-values of GNG/CG 304 with different structures were nearly the same at different punch speeds, and good formability of GNG/CG 304 was demonstrated. However, punch speed and microstructure needed to be optimized to avoid much lost of membrane strain region in biaxial stress state.

**Key words:** gradient nano-grained structure; deformation behavior; formability; ultrasonic impact treatment; AISI 304 stainless steel

## 1 Introduction

Nanocrystalline (NC) metallic materials have been reported to offer a variety of beneficial properties over the conventional coarse-grained counterparts because of the nanometer-sized grains with a large number of grain boundaries[1]. However, restricted by the current synthesis techniques, it is up to now still very difficult to fabricate dense 'ideal' bulk NC metals free of contamination and porosity. Meanwhile, most of these techniques are not adapted to synthesize bulk NC materials on an industrial scale due to limitations in terms of time, equipment and cost[2]. Additionally, NC metals are usually strong but brittle. Their ultra-high strength and hardness are achieved at the expense of their ductility, which is typically less than a few percent in terms of uniform elongation[3]. The brittleness of NC metals is a severe setback to their practical applications.

Actually, most failures of engineering materials take place on the surface, such as fatigue crack nucleation, corrosion and wear, *etc*. These failures are very sensitive to the structure and properties of the material surface. Thus, optimization of the surface microstructure and properties may effectively enhance the global behavior and particularly the service lifetime of materials[4]. The importance of the material surface and the attractive properties afforded by NC materials have led to the development of a new terminology called surface nanocrystallization (SNC)[5]. Alternatives to bulk NC materials can be materials with a NC surface layer, which is easier to produce and more cost-efficient. SNC could be achieved by many methods, and surface severe plastic deformation (SSPD) method has been considered as a simple but effective approach[6]. Gradient nano-grained (GNG) structure is formed on the top layer of metals with coarse grains (CG) (GNG/CG structure) by accumulation of plastic strain due to gradual decrease of the strain and strain rate along depth in the process of SSPD[7]. The chemical composition is not changed during this process and



(Received: Oct. 20, 2016; Accepted: May 18, 2017)

YANG Xinjun (杨新俊): Assoc. Prof.; Ph D; E-mail: xinjun_yang@163.com

*Corresponding author: WANG Wei(王伟): Assoc. Prof.; Ph D; E-mail: materials@whut.edu.cn

Funded by the National National Natural Science Foundation of China (No. 51505189), Open Project of Jiangsu Key Laboratory of Advanced Food Manufacturing Equipment & Technology (No. FM-2015-5)

good corrosion resistant is retained as well as the excellent interfacial bonding between the surface layer and the matrix.

The 300 series austenitic stainless steels (AASs) have been widely used in many fields, such as petroleum, chemical engineering, nuclear power generation and food processing because of their superior corrosion resistance and good formability[8]. One of the major drawbacks of AASs is their low strength in the annealed states, which limits their engineering applications with higher requirements[9]. However, a very limited number of techniques can be applied to strengthen AASs without compromising other useful properties for their special austenitic microstructure. Thus, with the emergence of SNC, new ways to improve the mechanical properties of materials have been developed. With regards to the Hall-Petch relationship, the GNG/CG structure could greatly enhance the strength of AASs[10].

Many techniques based on SSPD method have been successfully applied in achieving SNC in 300 series AASs, and grain refinement mechanism has been well investigated[11-14]. Tensile strength, thermal stability, fatigue limit, corrosion behavior of different kinds of AASs processed by different kinds of techniques, *e g,* SMAT (surface mechanical attrition treatment)[15,16], UNSM (ultrasonic nano-crystal surface modification)[17], LSP (laser shock peening)[18], UIT (ultrasonic impact treatment)[19], SP (shot peening)[20], FMRR (fast multiple rotation rolling)[21] and DR (deep rolling)[22], have also been investigated. Results revealed that the tensile strength, fatigue, wear and corrosion properties were improved obviously, but little information was available on the formability of GNG/CG AASs, which was very important for the fabrication of industrial devices with GNG/CG materials.

In this paper, the GNG layers with different microstructures were prepared on surfaces of the 304 austenitic stainless steels by ultrasonic impact treatment (UIT). UIT demonstrates good efficiency to induce SNC in AASs[12,19]. It is flexible, cost low and with excellent controllability which could be suitable for industrial applications. The formability of the GNG/CG 304 was experimentally investigated, and the influences of GNG structure on the deformation behaviors of GNG/CG 304 were also discussed.

## 2 Experimental

The material investigated in the experiments was the austenitic stainless steel AISI 304, with a composition (in mass %) of 0.058 C, 0.35 Si, 1.32 Mn, 0.032 P, 0.007 S, 17.45 Cr, 8.28 Ni and balance Fe. The pre treated state had initial grain size of the order of about 30 μm.

The UIT equipment was applied to achieve the GNG/CG structure on the surface of AISI 304. The frequency was about 21 kHz. The output power was between 0.9 to 1.5 kW, and the impact velocity was 5 m/s. More details were shown in Ref.[23]. Samples were divided into five groups with different coverage and numbered as 1, 2, 3, 4 and 5 in this paper. The coverage, reflecting the accumulation of plastic strain, is the ratio of treatment duration to time required for complete plastic deformation of the treated area. In this paper, the coverage was chosen as 30, 60, 90, 120 and 150, respectively, corresponding to different treatment durations (1, 2, 3, 4 and 5 min).

A ZEISS Axio Observer A1m optical microscope was used to measure the microstructure along the depth. The cross-sections were mechanically polished using silicon carbide paper to grade 2 000, then on a polishing cloth with a liquid suspension of 0.04 μm alumina, and finally etched at room temperature in a solution of 25 mL $HNO_3$ and 75 mL HCl. X-ray diffraction (XRD) analysis on the surface layer of the treated sample was carried out on a D/max 2500VL/PC Equipment X-ray diffractometer (6 kW) with CuKα radiation. Small angular steps of $2\theta = 0.02^{o}$ and a counting time of 2 s were used to measure the width of diffraction peak in the step-scanning mode. A standard $SiO_2$ sample was employed to calibrate the instrument and the average grain size was calculated from line broadening of Bragg diffraction peaks using the Williamson-Hall method as the following formula[24]:

$$\beta\cos\theta = \frac{K\lambda}{d} + 2\varepsilon\sin\theta \tag{1}$$

where $\beta$ is the peak width at half the maximum intensity, $\theta$ is the Bragg angle, $K$ is the Scherrer constant ($K = 0.9$), λ is the X-ray wavelength, $d$ is the crystallite size and $\varepsilon$ is the microstrain. Nanoindenter (XP, fitted with a Berkovich diamond indenter) was also applied to estimate the hardness, and the maximum load for the experiments was 500 nN.

The investigation on the deformation behavior in uniaxial stress state was carried out by tensile tests. The samples were of dog bone shape with 1 mm/5 mm thickness and the gauge length was 10 mm. Both sides of the sample were treated by UIT. The tensile strain

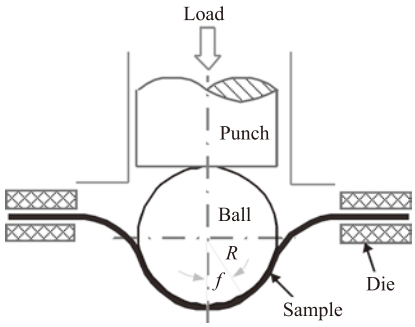


Fig.1 Schematic diagram of SPT

rate was $10^{-3}$ $s^{-1}$ and three samples were tested to ensure the repeatability. The small punch tests (SPTs) were used to investigate the deformation behavior and formability of GNG/CG 304 in biaxial stress state. The process of the test is illustrated in Fig.1. The SPT sample is a small disk with a diameter of 10 mm and a thickness of 0.5 mm. Different from the tensile test samples, the SPT samples were treated on one side. Three samples were also tested to ensure the repeatability. During the test, the sample was clamped in the center of the die, the ball contacted the untreated surface, and the load was applied to the sample from ball with a punch. Subsequently, the deflection of sample center and applied load were monitored and recorded by transducers during the deformation.

## 3 Results and discussion

### 3.1 Microstructures of UIT samples

Fig.2 is the optical image of the cross-section of sample 3. Three typical zones are formed after the treatment: A, Gradient nano-grained Layer; B, Severe plastic deformation band, and C, Plastic deformation Zone. Clear boundary exists between zones A and B, and the GNG layer has different etching pattern for the NC with large grain boundaries having different erosional characteristic[23]. The thickness of GNG layer with different coverage is estimated and presented in Fig.3. It is obvious that the thickness is nearly unchanged, when the coverage reaches 90.

Fig.4 illustrates the X-ray diffraction (XRD) patterns after the treatment with different coverage, and Fig.5 illustrates the grain size variation on the surface following the treatment. The grain size also decreases slightly when the coverage reaches 90, and the surface grain size tends to be about 20 nm when the coverage is over 90. The grain refinement mechanism of metals with low stacking fault energy (SFE) is the twin-twin self-intersection at high strain rate, and the thickness of twin lamella determines the final grain size. The critical

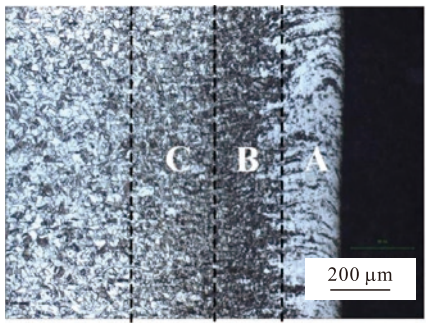


Fig.2 Section metallograph of sample 3

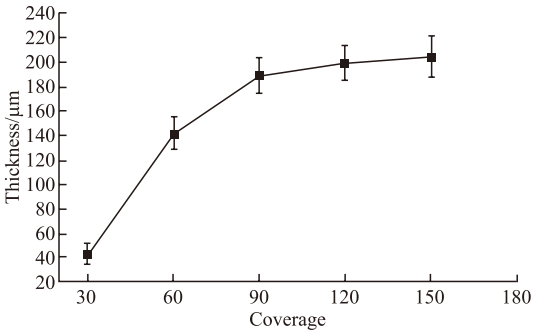


Fig.3 Thickness of GNG layer with different coverages

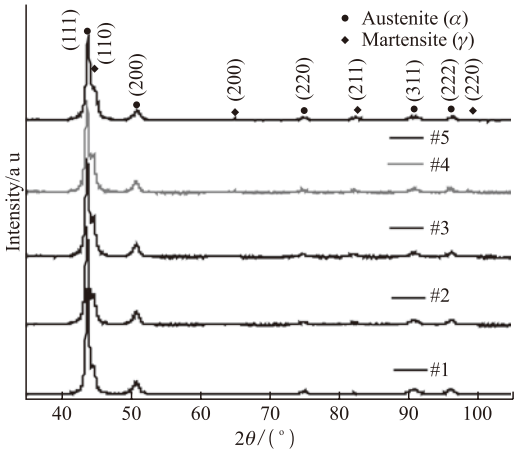


Fig.4 XRD patterns after the treatment

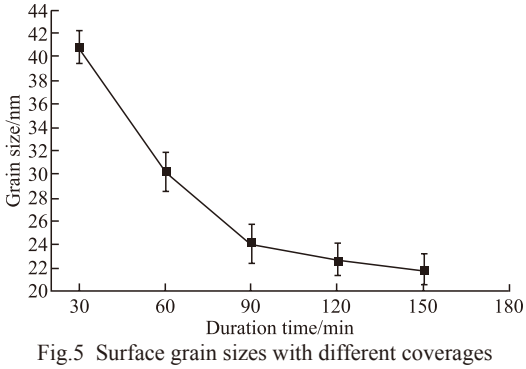


Fig.5 Surface grain sizes with different coverages

twin thickness ($\lambda_c$) depends on the twin boundary energy ($\gamma_{TB}$ ) and the driving stress of twin nucleation ($\sigma_T$) as the following formula[16]:

$$\lambda_c = \frac{5\pi}{4}\frac{G\gamma_{TB}}{\sigma_T^2} \quad (2)$$

And driving stress of twin nucleation, $\sigma_T$, can be given by:

$$\sigma_T = 6.13\frac{\gamma_{SFE}}{b_p} \quad (3)$$

where $b_p$ is the value of the Burgers vector of a Shockley partial dislocation, $G$ is the shear modulus and $\gamma_{SFE}$ is the stacking fault energy. For the 304 stainless steel, $\gamma_{SFE}$=16 mJ·m$^{-2}$, $b_p$ = 0.147 nm, and $\gamma_{TB} \geqslant 2\gamma_{SFE}$. So the minimum thickness of twin lamella is calculated to be 20 nm which is in accordance with the minimum surface grain size following the treatment. So it could be considered that the microstructure of GNG layer is stable and with slight variation when the coverage is larger than 90. Thus, the coverage of 30 to 90 is chosen as the input parameters of UIT to produce GNG/CG 304 stainless steel with different GNG structures.

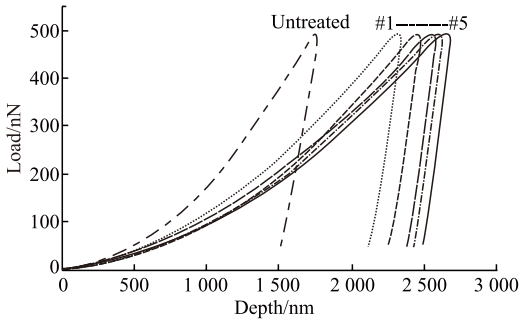


Fig.6 Nanoindentation load-depth curves

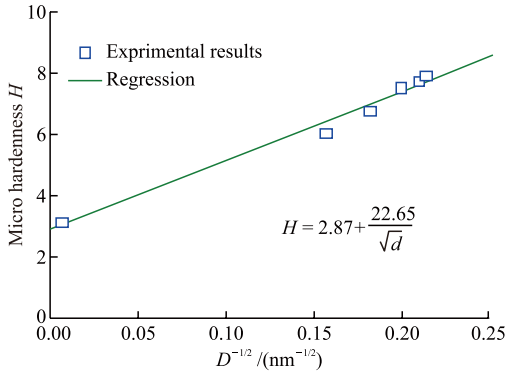


Fig.7 Microhardness varied with grain size on the surface

Fig.6 illustrates the nanoindentation load-depth curves on the surface of untreated sample and sample 1 to 5. According to the data obtained from Figs.5 and 6, it is found that the microhardness and grain size of the nanocrystalline 304 follow the Hall-Petch relation:

$$H = H_O + \frac{K_y}{\sqrt{d}} \quad (4)$$

where $H_O$ and $K_y$ are constants of 2.87 GPa and 22.87 GPa•nm$^{1/2}$, respectively (as shown in Fig.7).

### 3.2 Deformation behavior in uniaxial tensile stress state

In tensile tests, the 5 mm thick samples were treated with the coverage of 30, 60 and 90, respectively, while the 1 mm thick samples were treated with the coverage of 30 as a contrast to the SPTs mentioned in the next section. The tensile stress-strain curves of treated samples are shown in Fig.8, and the parameters of mechanical properties are listed in Table 1. Results show that the 0.2% offset yield strength $\sigma_{0.2}$ has been improved with the decrease of surface grain size and the increase of the GNG thickness (following *H-P* relationship). However, the $\sigma_{0.2}$ value of 1 mm thick sample is nearly 1.62 times compared with that of 5 mm thick sample processed with 30 coverage for the thicker sample having a smaller proportion of GNG layer over the whole sample. However, the ultimate tensile strength $\sigma_b$ is nearly unchanged after the treatment. It means that the accumulation of damage is not changed when the GNG layer is induced in 304, and nothing to do with the grain size and thicknesses of the GNG or CG layers. The elastic modulus of the sample has decreased after UIT processing. It is due to the residual stress profiles along the thickness of processed samples induced by UIT[25].

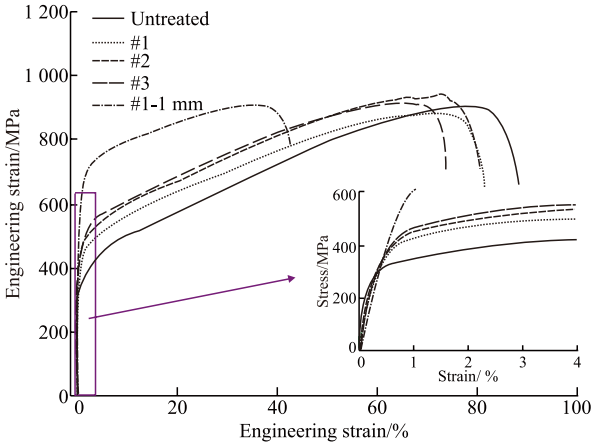


Fig.8 Stress-strain diagram of GNG/CG 304

On the other hand, as a result of the decrease of the surface grain size and the increase of the GNG thickness, the tensile elongation decreases by 8.3%, 11.0% and 17.6% for sample 1 to 3, respectively. The true strain to fracture $\varepsilon_{total}$ can be divided into two sub-strains, the uniform true strain before necking $\varepsilon_{unif}$ and the true strain after the onset of necking $\varepsilon_{neck}$. As summarized in Table 1, the uniform true strain before necking decreases from 0.55 for the untreated sample to 0.527, 0.516 and 0.484 respectively. However, the true

**Table 1 Mechanical property of different samples**

| Sample No. | Yield strength $\sigma_{0.2}$ / MPa | Ultimate tensile strength $\sigma_b$ / MPa | True strain to fracture $\varepsilon_{total}$ /% | Uniform true strain before necking $\varepsilon_{unif}$ /% | True strain after the onset of necking $\varepsilon_{neck}$ /% | Strain hardening exponent *n* |
|---|---|---|---|---|---|---|
| Untreated | 306 | 905 | 63.3 | 55.0 | 8.0 | 0.48 |
| #1 | 373 | 890 | 59.6 | 52.7 | 6.9 | 0.37 |
| #2 | 401 | 917 | 58.3 | 51.6 | 6.7 | 0.37 |
| #3 | 433 | 901 | 55.4 | 48.4 | 7.0 | 0.35 |
| #1-1 mm | 603 | 907 | 33.0 | 28.1 | 6.4 | 0.24 |

strain after the onset of necking changes little under the processing condition. The strain-hardening exponent *n* decreases after the treatment. Nevertheless, it is still could be accepted for the engineering applications, which means that GNG/CG 304 owns good strain hardening capacity.

It is not surprised that the strength of GNG/CG 304 stainless steel is improved evidently with small loss of ductility[23]. This is because AISI 304 with GNG/CG structure is elastically homogeneous but plastically gradient, and the strain localization of NC in GNG layer is effectively suppressed by the CG substrate. Fig.9 is the tensile fracture morphology of GNG/CG 304 with the coverage of 90. A typical ductile fractography expresses the good ductility of GNG/CG 304. Nanostructural layer on the surface can be distinguished from the matrix, and the sizes of dimples change of gradient from the treated surface to the matrix for the gradient plastic deformation of GNG/CG 304 in uniaxial stress state.

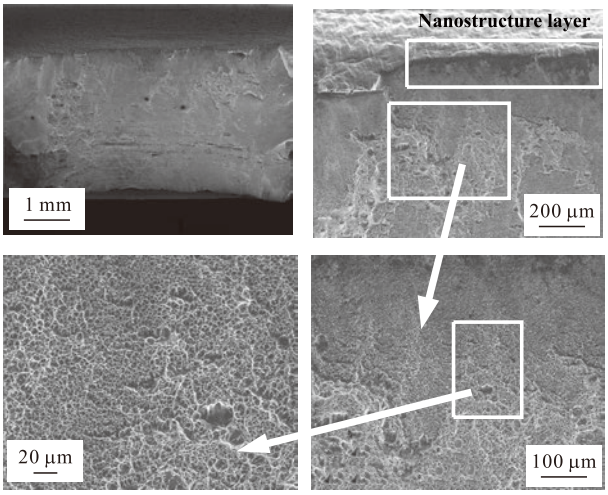


Fig.9 Fracture morphologies of GNG/CG 304

It is also pointed out in Ref.[17] that the tensile ductility of GNG/CG metals is limited by the CG substrate, and has no relation to the GNG layer. Based on this, it is reasonable that GNG/CG 304 with the thickness of 5 mm has a better ductility than the 1 mm-samples, because 5 mm-samples have thicker CG substrates. Plot of the thickness of substrate (*h*) *versus* uniform true strain before necking ($\varepsilon_{unif}$) is shown in Fig.10. An approximate linear relationship is illustrated, and it could be described by the following formula:

$$h = 0.012\,9\varepsilon_{unif} + 27.142 \tag{5}$$

According to the relationship, the ductility of GNG/CG 304 could be preliminarily estimated by its microstructure. It also provides a strategy for optimizing the microstructure of GNG/CG 304 to minimize the reduction in the ductility in uniaxial stress state.

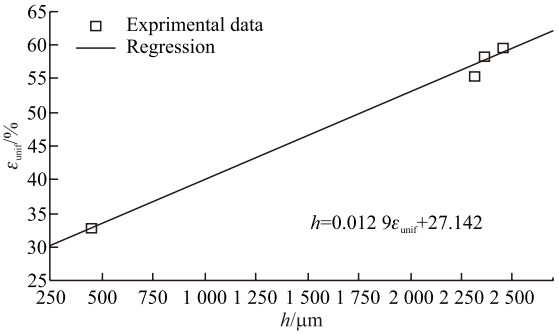


Fig.10 Thickness of substrate (*h*) *vs* uniform true strain before necking $\varepsilon_{unif}$

## 3.3 Deformation behavior and formability in biaxial stress state

The load - displacement (*L-D*) curves are exhibited in Fig.11. Typical stages depicting the behaviors of materials during deformation are marked on the curves. The first stage, elastic bending, is associated with the local surface microyielding. During the second stage, plastic bending, plastic flow begins and spreads within the sample-punch contact zone. Biaxial deformation of flat sample into a dome-shaped cap occurs during the next stage, membrane stretching. Once the maximum load capacity is reached, unstable plastic flow begins leading to the formation of cracks and sample failure[26]. The yield strength $\sigma_s$ and tensile strength $\sigma_b$ can be determined by the following two equations:

$$\sigma_s = \alpha\left(p_y / t_0^2\right) \tag{6}$$

$$\sigma_b = a\left(p_m/t_0^2\right) - b \tag{7}$$

where $p_y$ is the elastic plastic transition load, $p_m$ is the maximum load, and $t_0$ is the sample thickness. $\alpha$, $a$ and $b$ are material parameters and equal to 0.36, 0.13 and 320 for AISI 304, respectively[27]. To estimate the equivalent strain induced in these small punch samples, the final thickness $t$ is measured over areas deformed under membrane stretching located at $\varphi$=20 to 45 deg with respect to the vertical axis of the dome as illustrated in Fig.1. The true strain $\varepsilon$ is estimated as[26]:

$$\varepsilon = \ln\left(t_0/t\right) \tag{8}$$

According to miniaturized Erichsen test, which is similar to SPT but with bigger tested sample, the first-order derivative of punch load ($F$) with respect to the displacement ($X$) can be calculated to distinguish the deformation stages from each other at SPT[28, 29]. The d$F$/d$X$-$X$ curves are depicted in Fig.12. The elastic deformation is a narrow region, which is not presented in the figure. The plastic bending is valid up to the point "a", the lowest d$F$/d$X$ value in the first stage of d$F$/d$X$-$X$ curves. The membrane stretching takes place between points "a" and "c", and the d$F$/d$X$ increases with increasing displacement ($X$). The transition of plastic deformation from biaxial bending into membrane strain is between points "a" and "b". After this point, d$F$/d$X$-$X$ curve slope becomes nearly steady and/or reflects a slight increase within the region between points "b" and "c". In this sub stage, the thickness of the sample decreases uniformly with the membrane strain[29,30]. A possible reduction in punch load is balanced by the strain hardening capacity of materials while the dome thickness is decreasing. Further deformation after point "c" causes deformation localization, and $L$-$D$ curves reach the peak load at point "d". Beyond this point, the punch load starts decreasing with crack initiation and propagation on the dome surface with further deformation.

The results of SPTs are summarized in Table 2. It is revealed that the yield strength $\sigma_s$ of untreated sample is 300 MPa which agrees well with $\sigma_{0.2}$ obtained from the tensile test. After UIT treatment with different coverage, $\sigma_s$ increases obviously. The maximum value of $\sigma_s$ is 803 MPa for sample 3, which is 168% over the untreated one. Considering the different thicknesses between the tensile and SPT samples, the rule of mixtures (ROMs) of Voigt is employed to compare the yield strength of GNG samples with different thicknesses[31]. The results show that GNG/CG 304 with the same thicknesses has the same yield strength values at both uniaxial tensile and biaxial loads. Similar to the results in the tensile test, the ultimate tensile strength $\sigma_b$ is nearly the same before and after the treatment at SPTs. Additionally, it is independent on the thickness of GNG/CG sample and approximate to the value of the corresponding samples obtained from the tensile tests.

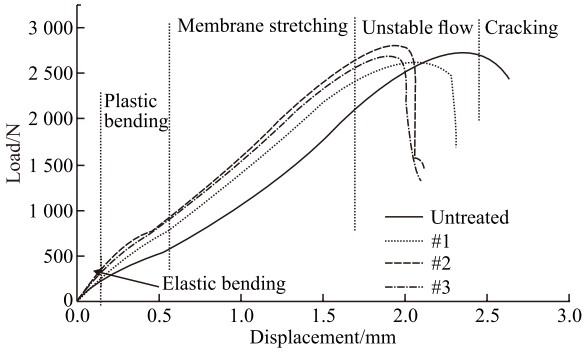


Fig.11 *L-D* curves of GNG/CG 304

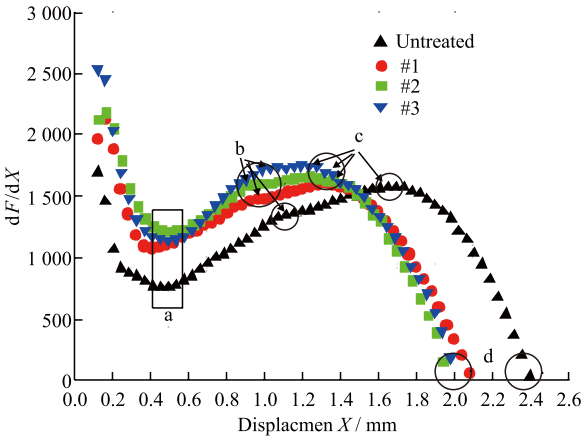


Fig.12 d$F$/d$X$ *vs* $X$ curves of GNG/CG 304

**Table 2 Mechanical properties of different samples in SPT**

| Sample No. | Yield strength $\sigma_{0.2}$ / MPa | Tensile strength $\sigma_b$ / MPa | True strain $\varepsilon$ |
|---|---|---|---|
| Untreated | 302 | 993 | 67.9 |
| #1 | 610 | 954 | 57.9 |
| #2 | 704 | 1 024 | 50.9 |
| #3 | 807 | 966 | 50.1 |

The Erichsen index (Ei) is used to estimate the formability of material in biaxial stress state, and it is equal to the value of displacement before point "d". From Fig.12, it could be found that the grain size and thickness of GNG layer have little effect on the Ei-value. The GNG/CG 304 treated with different coverage has similar Ei-value, which decreases by about 16.7% over CG 304. The region between "b" and "c" indicated

as membrane strain region is related to the strain-hardening capacity of tested material. Displacement in this region decreases with decreasing surface grain size and increasing thickness of GNG layer, which is about 0.6 mm for untreated sample, and 0.5, 0.4, 0.25 mm for samples 1-3, respectively. Meanwhile, the ratio of membrane strain displacement to Ei is about 25% for untreated sample and sample 1. Then it drops to 20%, 12.5% for samples 2 and 3. According to Ref. [28], this ratio determines the proportion of uniform elongation to elongation to failure. Compared with the results obtained from 1 mm tensile sample, GNG/CG 304 indicates better ductility in biaxial stress state and a high strain hardening may occur during the secondary deformation processes like deep drawing[29]. After point "d", the initiation and propagation of cracks start and result in the final fracture of SPT samples. However, sample 2 has longer fracture displacement compared with samples 3 and 4. It may be that high energy state of the NC grain boundaries and martensite content of GNG/CG 304 exceed critical values, then the crack propagation rates enhance rapidly in biaxial stress state, when the coverage reaches 60. The final true strain decreases by 14.7% over untreated sample for sample 1 and 25.0% for samples 2 and 3 as shown in Table 2. Connected with Fig.12, it could be proved that the fractural displacement in SPT has some relationship with the equivalent strain. So samples 2 and 3 have similar fractural displacement and final true strain.

Compared with the $\varepsilon_{\text{total}}$ obtained from 1 mm GNG/CG 304 sample in tensile test, the final true strain of sample 1 in SPT is 55.3 %, and increases by 68.8% over tensile sample. Thus, it is reasonable to conclude again that GNG/CG materials exhibit excellent ductility under biaxial load in comparison with the uniaxial load. This may be attributed to the stress triaxiality $T$, indicated by Eq.(9), which plays an important role in plastic deformation of ultrafine-grained (UFG) and nano-grained metallic materials:

$$TF = \frac{\sigma_m}{\bar{\sigma}} = \frac{(\sigma_{xx} + \sigma_{yy} + \sigma_{zz})/3}{\sqrt{[(\sigma_{xx} - \sigma_{yy})^2 + (\sigma_{yy} - \sigma_{zz})^2 (\sigma_{xx} - \sigma_{zz})^2]/2}} \tag{9}$$

where $\sigma_s$ is the hydrostatic stress, $\bar{\sigma}$ is Mises stress. In the SPT, $\sigma_{zz}$ is equal to zero for the point on the down surface (nano surface layer) of the tested specimens. So:

$$TF = \frac{\sigma_m}{\sigma_{eq}} = \frac{2/3 \cdot \sigma_{xx}}{\sigma_{xx}} = \frac{2}{3} \tag{10}$$

$T$ with high value can trigger microshear banding and promote the GB migration and slip processes of UFC and NC materials[26], which provide substantially all contribution to plastic deformation, and result in the growth of nano-sized grains[7]. Fig.13 shows the nanoindentation load-depth curves on GNG layer surface at necking and homogeneous regions in tensile test and contact region in SPT, respectively. According to Eq.(4), the grain sizes were estimated. The nano-sized grains on the surface grow from about 40 to 220 nm in SPT, while the grain size is about 80 and 150 nm at necking and homogeneous regions in tensile test.

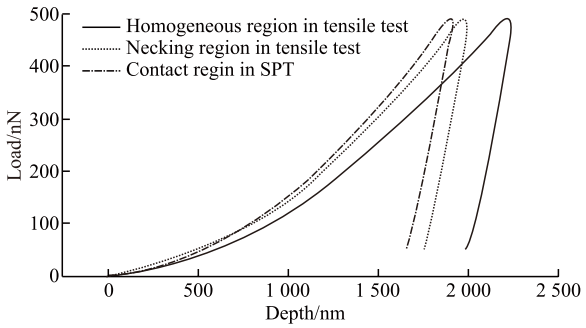


Fig.13 Nanoindentation load-depth curves after the tests

$T$ increases in the necking region ($T$>1/3), while $T$ is equal to 1/3 in homogeneous tensile deformation stage. Increase of $T$ helps GNG /CG 304 having similar true strain after the onset of necking $\varepsilon_{\text{neck}}$ compared with untreated one. In the region of biaxial stretching of small punch sample, $T$ is equal to 2/3 which exceeds the $T$-value in the necking region of tensile sample, thus leading to a better ductility than that of the uniaxial tensile sample.

Figs.14 and 15 are the fractographes of tensile test and SPT samples. Dimples are formed in the surface layer of GNG/CG 304 in SPT (shown by arrow in Fig.14(b)), instead of smooth fracture presented on the surface of GNG/CG 304 in tensile test (showed by arrow in Fig.15(b)). Better ductility of GNG/CG 304 in biaxial stress state is also proved by the comparison. This is a good signal for the engineering applications of GNG/CG 304, because the materials are in multiaxial stress state during the manufacture and service of industrial devices.

The effect of punch speed on the formability of GNG/CG 304 in biaxial stress state is shown in Figs.16 and 17. The punch speeds are 0.3, 0.5, 1 and 3 mm/

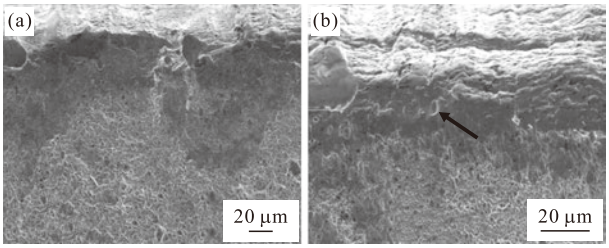

Fig.14 Surface layer fracture morphologies of tensile test sample

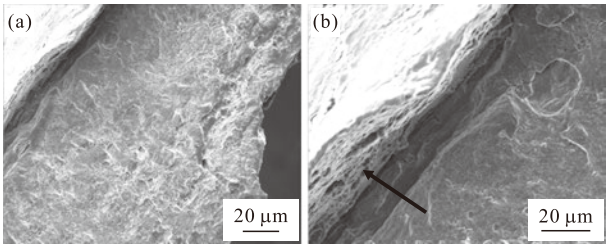

Fig.15 Surface layer fracture morphologies of SPT sample

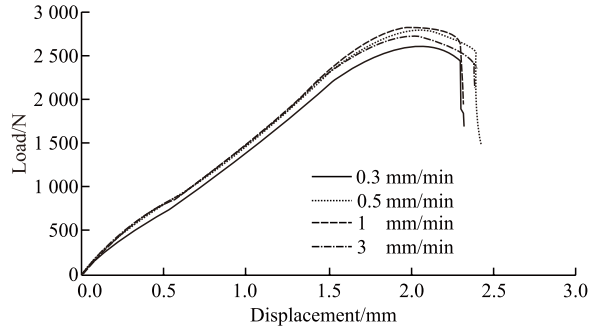

Fig.16 *L-D* curves at different punch speeds

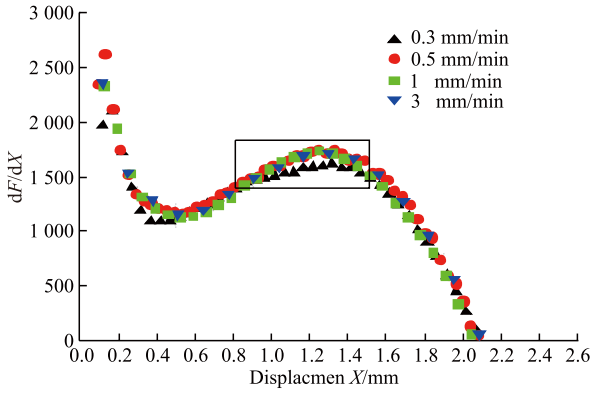

Fig.17 d*F*/d*X vs X* curves at different punch speeds

min, respectively. The *L-D* curves arise. But the Ei-value and true strain are nearly unchanged at elevated punch speeds. However, the displacement of membrane strain disappears when the punch speed is higher than 0.3 mm/min. It has been revealed that the strain rate sensitivity of GNG/CG 304 is about 40 times over CG 304[23]. The high strain rate sensitivity brings high flow stress. It may extend the region of transition of plastic deformation from biaxial bending into membrane strain and remove the displacement of membrane straining. Nevertheless, inside the strain localization region, high strain rate induced by elevated punch speed would offer more resistance to necking down. It would extend the displacement of deformation localization[32]. During the forming process, membrane strain region is important. The deformation speed needs to be well controlled to avoid the disappearance of membrane strain in biaxial stress state.

## 4 Conclusions

The GNG top layer was fabricated on CG AISI 304 by UIT, and the coverage of 30 to 90 was chosen as the input parameters to produce GNG/CG 304 with different GNG structures. The deformation behavior and formability of GNG/CG AISI 304 stainless steel in uniaxial and biaxial states have also been investigated by means of tensile tests and SPTs. The conclusions are shown as follows:

a) The gradient structure could coordinate the plastic deformation of GNG/CG 304, and the CG substrate could effectively suppress the strain localization of NC in GNG layer. An approximate linear relationship exists between the thickness of substrate ($h$) and uniform true strain before necking ($\varepsilon_{\text{unif}}$), and the ductility of GNG/CG 304 could be preliminary estimated by its microstructure in uniaxial stress state.

b) Grain growth of NC was observed during the plastic deformation which could promote the ductility of GNG/CG 304. High $T$-value improves the GB migration and slip in NC materials, and facilitates the grain growth processes. So better ductility of GNG/CG 304 in biaxial stress state in SPT, as well as similar true strain after the onset of necking $\varepsilon_{\text{neck}}$ compared with CG 304 in tensile test were revealed.

c) Grain size and thickness of GNG layer have little effect on the Ei-value, which decreases by about 16.7% over CG 304. The ratio of membrane strain displacement to Ei is about 25% for untreated sample and sample 1. Then it drops slightly for samples 2 and 3. The final true strain of sample 1 in SPT is 55.3 % with the increase of 68.8% over 1 mm GNG/CG 304 sample in tensile test, and dimples are formed in the surface layer. GNG/CG 304 demonstrates good formability and better ductility in SPT.

d) Ei-value and true strain are nearly unchanged at elevated punch speeds. The high strain rate sensitivity of GNG/CG 304 would extend the transition region and deformation localization region. However, the displacement of membrane strain is removed when the punch speed is higher than 0.3 mm/min. The

deformation speed needs to be well controlled to avoid the disappearance of membrane strain in biaxial stress state.

## References


[1] Ding Shui, Lv H G, Zhang K F. Superplasticity and Superplastic Bulging Behavior of ZrO2 /Ni Nanocomposite[J]. *J. Wuhan University of Technology-Mater. Sci. Ed.*, 2011, 26(1): 56-60

[2] Tao N R, Wang Z B, Tong W P, *et al*. An Investigation of Surface Nanocrystallization Mechanism in Fe Induced by Surface Mechanical Attrition Treatment[J]. *Acta Mater.*, 2002, 50(18): 4 603-4 616

[3] Gleiter H. Nanocrystalline Materials[J]. *Prog. Mater. Sci*., 1989, 33(4): 223-315

[4] Lu K, Lu J. Nanostructured Surface Layer on Metallic Materials Induced by Surface Mechanical Attrition Treatment[J]. *Mater. Sci. Eng. A*, 2004, 375-377(1): 38-45

[5] Lu K, Lu J. Surface Nanocrystallization (SNC) of Metallic Materials-Presentation of the Concept Behind a New Approach[J]. *J. Mater. Sci. Technol*., 1999, 15(3):193-197

[6] Valiev R Z, Korznikov A V, Mulyukov R R. Structure and Properties of Ultrafine-Grained Materials Produced by Severe Plastic Deformation[J]. *Mater. Sci. Eng. A*, 1993, 168(2):141-148

[7] Fang T H, Li W L, Tao N R, *et al*. Revealing Extraordinary Intrinsic Tensile Plasticity in Gradient Nano-Grained Copper[J]. *Science*, 2011, 331(6 024): 1 587-1 590

[8] Chen W Y, Zhou J. Preparation and Characterization of Stainless Steel/ TiC Nanocomposite Particles by Ball-milling Method[J]. *J. Wuhan University of Technology-Mater. Sci. Ed*., 2011, 24(1): 38-41

[9] Liu G Z, Tao N R, Lu K. 316L Austenite Stainless Steels Strengthened by Means of Nano-scale Twins[J]. *J. Mater. Sci. Technol*., 2010, 26(4): 289-292

[10] Kashyap B P. Towards Interrelationship of Grain Size, Cell Parameters and Flow Stress in Type 316L Stainless Steel[J]. *Acta Mater*., 2002, 50(9): 2 413-2 427

[11] Zhang H W, Hei Z K, Liu G, *et al*. Formation of Nanostructured Surface Layer on AISI 304 Stainless Steel by Means of Surface Mechanical Attrition Treatment[J]. *Acta Mater*., 2003, 51(7):1 871-1 881

[12] Lu J Z, Luo KY, Zhang Y K, *et al*. Grain Refinement Mechanism of Multiple Laser Shock Processing Impacts on ANSI 304 Stainless Steel[J]. *Acta Mater.*, 2010, 58(16): 5 354-5 362

[13] Mordyuk B N, Milman Y V, Iefimov M O, *et al*. Characterization of Ultrasonically Peened and Laser-shock Peened Surface Layers of AISI 321 Stainless Steel[J]. *Surf. Coat. Technol*., 2008, 202(19): 4 875-4 883

[14] Liu S, Gao S Y, Zhou Y F, *et al*. A Research on the Microstructure Evolution of Austenite Stainless Steel by Surface Mechanical Attrition Treatment[J]. *Mater. Sci. Eng. A*, 2014, 617: 127-138

[15] Roland T, Retraint D, Lu K, *et al*. Fatigue Life Improvement through Surface Nanostructuring of Stainless Steel by Means of Surface Mechanical Attrition Treatment[J]. *Scripta Mater.*, 2006, 54(11): 1 949-1 954

[16] Chan H L, Ruan H H, Chen A Y, *et al*. Optimization of the Strain Rate to Achieve Exceptional Mechanical Properties of 304 Stainless Steel Using High Speed Ultrasonic Surface Mechanical AttritionTreatment[J]. *Acta Mater.*, 2010, 58(15): 5 086-5 096

[17] Ye C, Telang A, Gill A S, *et al*. Gradient Nanostructure and Residual Stress Induced by Ultrasonic Nano-crystal Surface Modification in 304 Autensitic Stainless Steel for High Strength and High Ducility[J]. *Mater. Sci. Eng. A*, 2014, 613: 274-288

[18] Lu J Z, Qi H, Luo K Y, *et al*. Corrosion Behaviour of AISI 304 Stainless Steel Subjected to Massive Laser Shock Peening Impacts with Different Pulse Energies[J]. *Corros. Sci.*, 2014, 80: 53-59

[19] Mordyuk B N, Prokopenko G I, Vasylyev M A, *et al*. Effect of Structure Evolution Induced by Ultrasonic Peening on the Corrosion Behavior of AISI-321 Stainless Steel[J]. *Mater. Sci. Eng. A*, 2007, 458(1): 253-261

[20] Wang T, Yu J, Dong B. Surface Nanocrystallization Induced by Shot Peening and Its Effect on Corrosion Resistance of 1Cr18Ni9Ti Stainless Steel[J]. *Surf. Coat. Technol*., 2006, 200(16-17): 4 777-4 781

[21] Chui P, Suna K, Suna C, *et al*. Effect of Surface Nanocrystallization Induced by Fast Multiple Rotation Rolling on Hardness and Corrosion Behavior of 316L Stainless Steel[J]. *Appl. Surf. Sci.*, 2011, 257(15): 6 787-6 791

[22] Nikitin I, Altenberger I. Comparison of the Fatigue Behavior and Residual Stress Stability of Laser-shock Peened and Deep Rolled Austenitic Stainless Steel AISI 304 in the Temperature Range 25-600 °C[J]. *Mater. Sci. Eng. A*, 2007, 465(1): 176-182

[23] Yang X J, Wang X Y, Ling X, *et al*. Enhanced Mechanical Behaviors of Gradient Nano-grained Austenite Stainless Steel by Means of Ultrasonic Impact Treatment[J]. *Results Phys*., 2017, 7: 1 412-1 421

[24] Sekkal A C, Langlade C, Vannes A B. Tribologically Transformed Structure of Titanium Alloy (TiAl6V4) in Surface Fatigue Induced by Repeated Impacts[J]. *Mater. Sci. Eng. A*, 2005, 393(1-2):140-146

[25] Li J, Chen S, Wu X, *et al*. The Main Factor Influencing the Tensile Properties of Surface Nano-crystallized Graded Materials[J]. *Mater. Sci. Eng. A*, 2010, 527(26):7 040-7 044

[26] Moreno-Valle E C, Monclus M A, Molina-Aldareguia J M, *et al*. Biaxial Deformation Behavior and Enhanced Formability of Ultrafine-Grained Pure Copper[J]. *Metall. Mater. Trans. A*, 2013, 44(5): 2 399-2 408

[27] Mao X, Takahashi H. Development of a Further Miniaturized Specimen of 3 mm Diameter for TEM Disk Small Punch Test[J]. *J. Nucl. Mater.*, 1987, 150(1):42-45

[28] Saray O, Purcek G, Karaman I, *et al*. Improvement of Formability of Ultrafine-grained Materials by Post-SPD Annealing[J]. *Mater. Sci. Eng. A*, 2014, 619: 119-128

[29] Saray O, Purcek G, Karaman I, *et al*. Formability of Ultrafine-grained Interstitial-free Steels[J]. *Metall. Mater. Trans. A*, 2013, 44(9): 4 194-4 206

[30] Saray O. Biaxial Deformation Behavior and Formability of Precipitation Hardened Ultra-fine Grained (UFG) Cu-Cr-Zr Alloy[J]. *Mater. Sci. Eng. A*, 2016, 656: 120-129

[31] Li J J, Soh A K. Modeling of the Plastic Deformation of Nanostructured Materials with Grain Size Gradient[J]. *Int. J. Plast*., 2012, 39(4):88-102

[32] Wang Y M, Ma E. Three Strategies to Achieve Uniform Tensile Deformation in a Nanostructured Metal[J]. *Acta Mater*., 2004, 52(6): 1 699-1 709